IEEE Photonics Journal
An IEEE Photonics Society Publication

Open Access

Second-Order Intensity-Correlated Imaging Through the Scattering Medium

Volume 9, Number 6, Deccember 2017

Zhan Lei
Chunfang Wang
Dawei Zhang
Luxiao Wang
Wenlin Gong

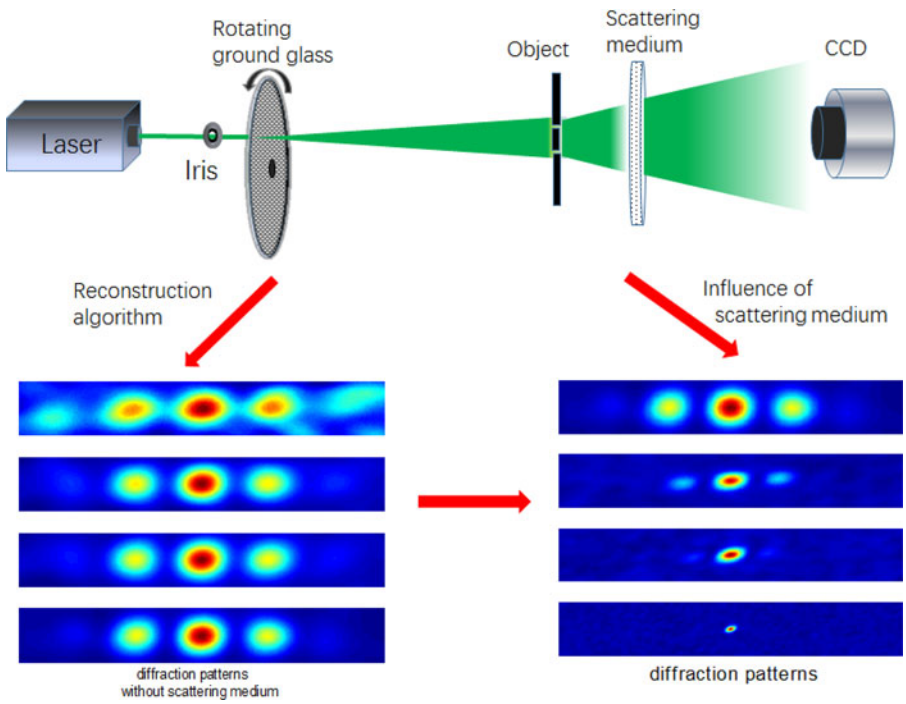

DOI: 10.1109/JPHOT.2017.2772265
1943-0655

IEEE photonics SOCIETY

IEEE

Second-Order Intensity-Correlated Imaging Through the Scattering Medium

Zhan Lei,[1] Chunfang Wang,[1] Dawei Zhang,[2] Luxiao Wang,[3] and Wenlin Gong[4]

[1]Department of Physics, University of Shanghai for Science and Technology, Shanghai 200093, China
[2]School of Optical-Electrical and Computer Engineering, University of Shanghai for Science and Technology, Shanghai 200093, China
[3]Chongqing Environmental Protection Information Center, Chongqing 401147, China
[4]Key Laboratory for Quantum Optics and Center for Cold Atom Physics of CAS, Shanghai Institute of Optics and Fine Mechanics, Chinese Academy of Sciences, Shanghai 201800, China

DOI:10.1109/JPHOT.2017.2772265

Manuscript received September 6, 2017; revised November 1, 2017; accepted November 6, 2017. Date of publication November 10, 2017; date of current version November 22, 2017. This work was supported in part by the Natural Science Foundation of China under Grants 11104185, 61378060, and 61571427, in part by Hi-Tech Research and Development Program of China (2013AA122901), and in part by Youth Innovation Promotion Association CAS (2013162). Corresponding authors: Wenlin Gong (gongwl@siom.ac.cn) and Chunfang Wang (e-mail:cfwang@usst.edu.cn).

Abstract: For a Hanbury Brown and Twiss system, second-order intensity-correlated imaging through the scattering medium is studied based on a new reconstruction algorithm. The analytical results, which are backed up by numerical simulation and experiments, demonstrate that the imaging quality decreases with the increase of the distance between the object and the scattering medium. Additionally, the new reconstruction algorithm is utilized to decrease the sampling number and improve the imaging efficiency.

Index Terms: Image processing, coherence imaging, quantum optics, photon statistics.

1. Introduction

Correlated imaging is an imaging technique that reconstructs an unknown object by measuring the second-order correlation between two light fields [1]–[6]. There are mainly two imaging modes for correlated imaging: ghost imaging and ghost diffraction. For both the two imaging modes, sampling number is a major factor that influences the imaging quality. How to get high-quality image with fewer samples is a very important topic in correlated imaging. In recent years, compressive sampling (CS), as an advanced image reconstruction algorithm, has been applied to ghost imaging, which can decrease the sampling number effectively [7], [8]. However, the image reconstruction is complicated and time-consuming.

For a realistic imaging system, imaging quality is also easily influenced by various environmental factors. It has been demonstrated that the effect of atmospheric turbulence, or scattering medium on the imaging quality of ghost imaging can be minimized to some extent [9]–[16]. In addition, ghost diffraction can overcome the influence of relative motion between the object and the detection system on the imaging resolution, and motion de-blurring is also demonstrated to be effective in a Hanbury Brown and Twiss (HBT) system [17], [18]. However, the influences of scattering on the imaging qualities of both ghost diffraction and the HBT system are not explored.

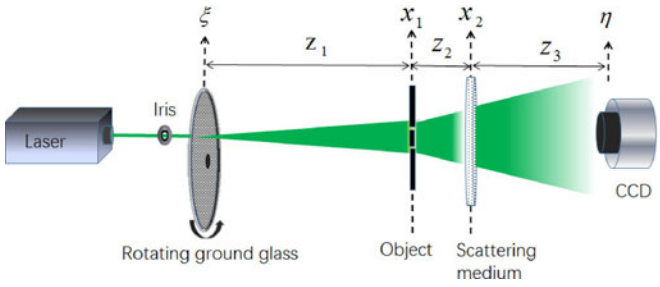

Fig. 1. The schematic of the experiment. CCD: charge-coupled device camera. The rotating ground glass is driven by a stepper motor. The iris, which is placed in front of the rotating ground glass, can continuously change the diameter of the laser beam from 1 to 12 mm. ξ, x_1, x_2, η are the transverse coordinates at the source plane, the object plane, the scattering plane, and the detection plane, respectively.

Compared with ghost diffraction, the structure of the HBT is simpler, and it has a higher precision in optical measurements [19]. Here we investigate the effect of the scattering medium on second-order intensity-correlated imaging in an HBT system. Meanwhile, a new reconstruction algorithm is proposed to decrease the sampling number and improve the imaging efficiency.

The paper is organized as follows. In Section 2, we theoretically analyze the influence of the scattering medium on second-order intensity-correlated imaging in an HBT system. In Section 3, a new reconstruction algorithm is proposed to decrease the sampling number and improve the imaging efficiency. In Section 4, using the new reconstruction algorithm, we give the numerical simulation and experimental results of second-order intensity-correlated imaging through the scattering medium in an HBT system. In Section 5, the summary is given.

2. Experimental Setup and Theoretical Analysis

The experimental schematic of second-order intensity-correlated imaging through the scattering medium is shown in Fig. 1. The pseudo-thermal light source is generated by passing a laser beam (the wavelength $\lambda = 532$ nm) through a rotating ground glass disk [5], [18]. The light field propagates a distance z_1 and then goes through an object. A random phase screen (a 2-mm-thick one-side frosted glass) acts as the scattering medium [20], [21], which is located at a distance z_2 behind the object. The light field transmitted through the scattering medium is recorded by a CCD camera. The distance between the scattering medium and the detection plane is z_3.

According to optical coherence theory, we can obtain the second-order correlation function on the detection plane [4]:

$$\Delta G^{(2,2)}(\eta_1, \eta_2) \propto \left| G^{(1,1)}(\xi_1, \xi_2) \times \left\langle \int d\xi_1 d\xi_2 h_1(\xi_1, \eta_1) h_2^*(\xi_2, \eta_2) \right\rangle \right|^2, \tag{1}$$

where $\langle \cdot \rangle$ denotes the ensemble average of a function, $G^{(1,1)}(\xi_1, \xi_2)$ is the first-order correlation function on the source plane, $h_1(\xi_1, \eta_1)$ is the impulse response function between the source plane and the detection plane, and $h_2^*(\xi_2, \eta_2)$ denotes the phase conjugate of the impulse response function between the two planes.

Assuming that the light field on the ground glass plane is fully spatially incoherent and the intensity distribution is uniform as a constant intensity I_0, then

$$G^{(1,1)}(\xi_1, \xi_2) \propto I_0 \delta(\xi_1 - \xi_2), \tag{2}$$

where $\delta(x)$ is the Dirac delta function.

For the schematic shown in Fig. 1, under the paraxial approximation, the impulse response function $h(\xi, \eta)$ between the source plane and the detection plane can be expressed as

$$h(\xi,\eta) \propto \int dx_1 dx_2 \exp\left\{\frac{jk}{2z_1}(x_1-\xi)^2\right\} \times T(x_1) \exp\left\{\frac{jk}{2z_2}(x_2-x_1)^2\right\} \times \exp\{j\phi(x_2)\} \times \exp\left\{\frac{jk}{2z_3}(\eta-x_2)^2\right\}, \tag{3}$$

where $k = 2\pi/\lambda$, $T(x_1)$ denotes the transmission function of the object, and $\phi(x_2)$ represents the phase shift of the random phase screen. According to the statistical property of the random phase screen, we can get the spatial autocorrelation function [22]

$$\Gamma(x_2, x_2') = \left\langle \exp\left\{j\left[\phi(x_2) - \phi(x_2')\right]\right\}\right\rangle = \exp\left\{-\sigma^2\left[1 - e^{-\frac{(x_2-x_2')^2}{s^2}}\right]\right\}, \tag{4}$$

where σ^2 is the variance of ϕ, and s is a constant associated with the autocorrelation function of the phase. If the source is large enough, substituting Eqs. (2)–(4) into Eq. (1), the correlation function is

$$\Delta G^{(2,2)}(\eta_1,\eta_2) \propto \left| \int dx_1 dx_2 dx_2' \Gamma(x_2, x_2') \times |T(x_1)|^2 \exp\left\{\frac{jk}{z_2}(x_2 - x_2')x_1\right\} \times \exp\left\{\frac{jk}{z_3}\left[\frac{z_2+z_3}{2z_2}({x_2}^2 - {x_2'}^2) + x_2'\eta_2 - x_2\eta_1\right]\right\}\right|^2. \tag{5}$$

If we set $z_2 + z_3 = z$ and $\eta_2 = 0$,

$$\Delta G^{(2,2)}(\eta_1, \eta_2 = 0) \propto \left|\mathcal{F}[f(x_2)]\right|^2_{\omega=\frac{2\pi\eta_1}{\lambda(z-z_2)}}, \tag{6}$$

where

$$f(x_2) = \int dx_2' \Gamma(x_2, x_2') \mathcal{F}\left\{\left|T\left(\frac{2\pi}{\lambda z_2}(x_2 - x_2')\right)\right|^2\right\} \times \exp\left\{\frac{jkz}{2z_2(z-z_2)}({x_2}^2 - {x_2'}^2)\right\}, \tag{7}$$

$\mathcal{F}\{\cdots\}$ denotes the Fourier transform of a function. From Eqs. (6) and (7), we can see that the distance z_2 has an effective influence on the diffraction pattern obtained by second-order intensity-correlated imaging with pseudo-thermal light. Due to the presence of the scattering medium, we obtain the Fourier transform of a new function $f(x_2)$ rather than the object transmittance function $T(x_1)$. It is reasonable to consider $f(x_2)$ as a new object function, which is related closely with the original object transmittance function $T(x_1)$.

3. Reconstruction Algorithm

Before presenting the results of second-order intensity-correlated imaging through the scattering medium, we propose a new reconstruction algorithm to decrease the sampling number. For the schematic shown in Fig. 1, the diffraction pattern can be obtained by calculating the second-order intensity fluctuation correlation function

$$\Delta G^{(2,2)}(\eta_1, \eta_2 = 0) = \frac{1}{K}\sum_{m=1}^{K} I_{1m}(\eta_1) I_{2m}(\eta_2) - \frac{1}{K^2}\sum_{m=1}^{K} I_{1m}(\eta_1) \sum_{m=1}^{K} I_{2m}(\eta_2), \tag{8}$$

where K is the total sampling number, $I_{1m}(\eta_1)$ is the intensity distribution of the mth sample, and $I_{2m}(\eta_2)$ is the intensity of the central point in the mth sample. If the sampling area recorded by the CCD camera is larger than the effective area occupied by the object's diffraction pattern, more independent measurements can be obtained from a sample by dividing it. Assuming that every

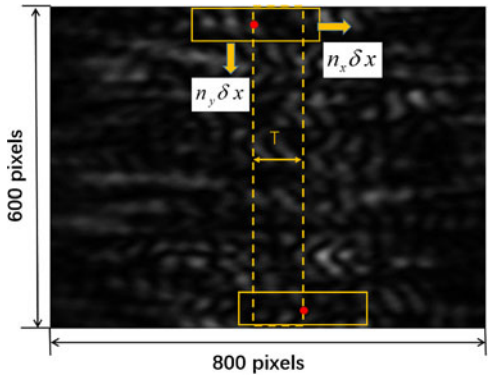

Fig. 2. Illustration of dividing a speckle pattern. The size of the speckle pattern is 800 × 600 pixels. The upper and bottom solid rectangle area denote the first measurement and the last measurement, respectively. The red dot denotes the center of the solid rectangle area. The dashed rectangle represents the central area of the speckle pattern with width T.

sample can be divided to L measurements, Eq. (8) can be rewritten as

$$\Delta G^{(2,2)}(\eta_1', \eta_2' = 0) = \frac{1}{KL}\sum_{m=1}^{K}\sum_{n=1}^{L} I_{1mn}(\eta_1') I_{2mn}(\eta_2') - \frac{1}{(KL)^2}\sum_{m=1}^{K}\sum_{n=1}^{L} I_{1mn}(\eta_1')\sum_{m=1}^{K}\sum_{n=1}^{L} I_{2mn}(\eta_2'), \tag{9}$$

where $I_{1mn}(\eta_1')$ denotes the intensity distribution of the nth measurement in the mth sample, and $I_{2mn}(\eta_2')$ denotes the the central point intensity of the nth measurement in the mth sample. Eq. (9) is the core formula of the new reconstruction algorithm. Obviously, compared with the conventional algorithm (Eq. (8)), more independent measurements can be obtained through the new reconstruction algorithm with available sample number K. That indicates fewer samples may be enough to complete measurements, which can help to shorten the imaging time and improve the imaging efficiency.

An experiment based on the schematic shown in Fig. 1 is performed to verify the new reconstruction algorithm described above. The object is a double slit with slit width $a = 0.2$ mm, center-to-center separation $d = 0.5$ mm, and slit height $h = 2.0$ mm. The transmission aperture of the iris is set as $D = 2.0$ mm, and the distances listed in Fig. 1 are set as follows: $z_1 = 120$ mm, and $z_2 + z_3 = 150$ mm. The exposure time window for the CCD camera is set to be 30 ms, and the sampling frequency is 10 Hz. The pixel size of the CCD camera is 3.45 μ m × 3.45 μ m, and the size of the speckle pattern recorded by the CCD camera is 800 × 600 pixels. When no scattering medium exists, based on the diffraction theory, the half width of the single-slit diffraction central bright stripes is $T = \frac{\lambda}{a}(z_2 + z_3) \approx 400$ μ m (about 115 pixels). Following the definition of Ref. [23], the spatial transverse coherence length in the detection plane is $\delta x = \frac{\lambda}{D}(z_1 + z_2 + z_3) \approx 72$ μm (about 20 pixels). It's obvious that the sampling area is larger than that of the object's diffraction pattern. Therefore, more independent measurements can be obtained from a speckle pattern by dividing it. Fig. 2 illustrates how to divide a speckle pattern in the case of no scattering medium. The size of the first measurement area is 250 × 40 pixels (the upper solid rectangle area), then we obtain another measurement after the solid rectangle area moves rightwards or downwards with a distance $n\delta x$. The central point (the red dot) of every measurement area is always restricted to the dashed rectangle area (115 × 600 pixels). After calculation, $N_x = T/\delta x \approx 6$, $N_y = (600 - 40)$ pixels/20 pixels $+1 = 29$, and $L = N_x * N_y = 174$, namely, 174 measurements can be obtained from a sample. $n_x = 1, ..., N_x$ and $n_y = 1, ..., N_y$ represent the horizontal and the vertical coordinates respectively, which determine the central point positions of every measurement. Fig. 3 depicts the results of second-order intensity-correlated imaging based on different reconstruction algorithms

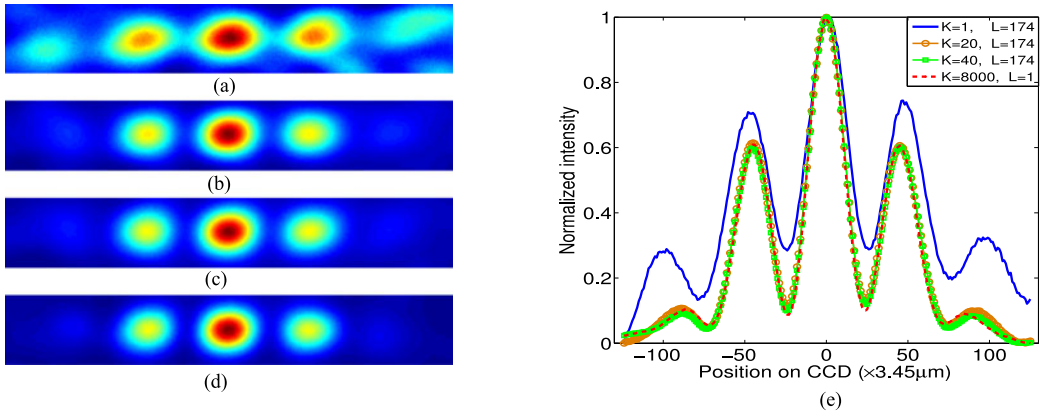

Fig. 3. Experimental results of second-order intensity-correlated imaging based on different reconstruction algorithms. (a–c) are the diffraction patterns achieved from the new reconstruction algorithm when K is 1, 20, and 40, respectively. (d) is the diffraction pattern achieved from the conventional reconstruction algorithm (8000 samples). (e) is the normalized intensity distributions corresponding to (a–d).

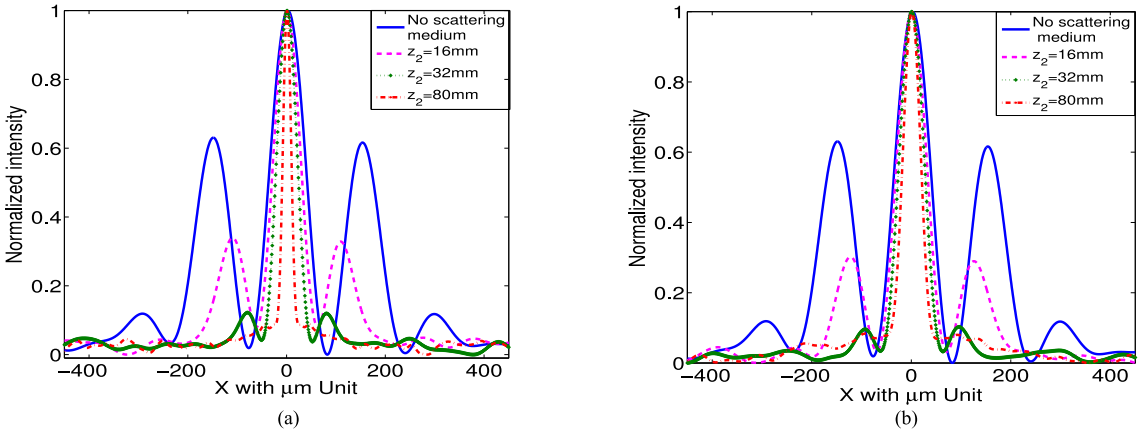

Fig. 4. Numerical simulation results of second-order intensity-correlated imaging in different positions of the scattering medium (40 samples). (a) $z_2 + z_3$ is fixed to 150 mm with different z_2. (b) z_3 is fixed to 150 mm with different z_2.

described above. (a–c) are the diffraction patterns achieved from the new reconstruction algorithm when the sampling number K is 1, 20, and 40, respectively. For comparison, the diffraction pattern obtained from the conventional reconstruction algorithm is shown in (d). It's obvious that the diffraction pattern (a) has a poor quality, while (b) and (c) are nearly the same as (d). To get a better view, the normalized intensity distributions corresponding to (a–d) are shown in (e). From Fig. 3, we can see that the diffraction patterns obtained from the new reconstruction algorithm are quickly convergent to that achieved from the conventional reconstruction algorithm. Therefore, we only need dozens of speckle patterns to complete sampling and obtain the diffraction pattern with high quality, and then the new reconstruction algorithm is applied to the simulation and the experimental process in Section 4.

4. Simulation and Experimental Results

In order to investigate the influence of the scattering medium on second-order intensity-correlated imaging, the numerical simulation and experimental results with different positions of the scattering medium are shown in Figs. 4 and 5, respectively. For comparison, the results in the case of no

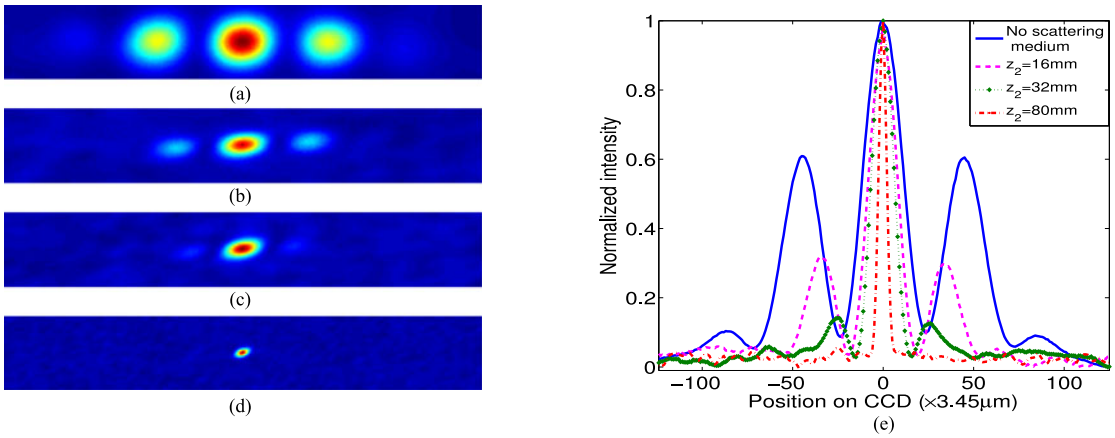

Fig. 5. Experimental results of second-order intensity-correlated imaging in different positions of the scattering medium ($z_2 + z_3 = 150$ mm, 40 speckle patterns). (a) is the diffraction pattern when no scattering medium exists. (b-d) are the diffraction patterns when z_2 is 16 mm, 32 mm, and 80 mm, respectively. (e) is the normalized intensity distributions corresponding to (a–d).

scattering medium are also shown in the figures. The distance z_1 and the object are the same as that in Section 3. Fig. 4(a) represents the numerical simulation results of different z_2 when $z_2 + z_3$ is fixed to 150 mm. Obviously, the high frequency decreases and moves toward the center as the scattering medium moves far away from the double slit. Combined with the analytical results (Eqs. (6)–(7)), we must make it clear that it is z_2, z_3 or both the two, that influences the diffraction pattern. Accordingly, Fig. 4(b) further demonstrates numerical simulation results of different z_2 when z_3 is fixed to 150 mm. It is observed that the high frequency moves more slowly toward the center as z_2 increases compared with the case of Fig. 4(a). The experimental results corresponding to Fig. 4(a) are shown in Fig. 5, in which (e) is the normalized intensity distributions corresponding to (a–d). Obviously, the scattering medium has an impact on the diffraction patterns. Compared with the results in the case of no scattering medium [see Fig. 5(a)], the qualities of the diffraction patterns degrade gradually and the high frequency information of the double slit can not be retrieved completely with the increase of z_2 [see Fig. 5 (b–d)], which is consistent with the numerical simulation results.

The results above show that the double slit information can be retrieved by the second-order intensity correlation at the expense of the imaging quality, which basically depends on the distance between the scattering medium and the double slit. Based on the theoretical analysis in Section 2, the influence of the scattering medium on the imaging quality can be explained as follows: according to the wave optics theory, as the distance between the scattering medium and the double slit increases, the interference effect of the double slit on the scattering plane becomes obvious. It is reasonable to consider that a new extended double slit is formed on the scattering plane, whose slit width can be approximately expressed as $a' \propto a + \frac{\lambda}{a} z_2$. When z_3 is fixed to 150 mm, the increase of z_2 leads to the increase of a', thus, as shown in Fig. 4(b), narrower envelope curve is formed on the basis of the diffraction theory. As a result, the high frequency decreases and moves toward the center. When $z_2 + z_3$ is fixed to 150 mm, as z_2 increases, the change of a' is the same as the case above and the magnification of the diffraction pattern is proportional to z_3. Therefore, as displayed in Fig. 4(a), the high frequency decreases and moves faster toward the center compared with the case of Fig. 4(b). It can be predicted that the high frequency will disappear when z_2 increases to some extent and the diffraction pattern eventually becomes a small circular spot.

5. Summary

In summary, a new reconstruction algorithm is proposed to obtain the diffraction pattern, which helps to shorten the sampling time and realize fast imaging. Using the new reconstruction algorithm, the

diffraction patterns can also be reconstructed with only dozens of samples even if there is scattering medium between the object plane and the detection plane. In addition, both the numerical simulation and experimental results show that the imaging quality decreases as the distance between the object and the scattering medium increases. This work can help to deepen the understanding of the second-order intensity-correlated imaging and will be of great benefit to the application of the correlated imaging through scattering medium.

References

[1] D. V. Strekalov, A. V. Sergienko, D. N. Klyshko, and Y. H. Shih, "Observation of two-photon ghost interference and diffraction," *Phys. Rev. Lett.*, vol. 74, no. 18, pp. 3600–3603, 1995.

[2] A. Gatti, E. Brambilla, M. Bache, and L. A. Lugiato, "Correlated imaging, quantum and classical," *Phys. Rev. A*, vol. 70, no. 1, pp. 013 802–1–013 802–10, 2004.

[3] M. H. Zhang *et al.*, "Lensless fourier-transform ghost imaging with classical incoherent light," *Phys. Rev. A*, vol. 75, no. 2, pp. 021 803–1–021 803-4, 2007.

[4] J. Cheng and S. S. Han, "Incoherent coincidence imaging and its applicability in x-ray diffraction," *Phys. Rev. Lett.*, vol. 92, no. 9, pp. 093 903–1–093 903-4, 2004.

[5] F. Ferri, D. Magatti, A. Gatti, M. Bache, E. Brambilla, and L. A. Lugiato, "High-resolution ghost image and ghost diffraction experiments with thermal light," *Phys. Rev. Lett.*, vol. 94, no. 18, pp. 183 602–1–183 602-4, 2005.

[6] A. Gatti, E. Brambilla, M. Bache, and L. A. Lugiato, "Ghost imaging with thermal light: Comparing entanglement and classical correlation," *Phys. Rev. Lett.*, vol. 93, no. 9, pp. 093 602–1–093 602-4, 2004.

[7] O. Katz, Y. Bromberg, and Y. Silberberg, "Compressive ghost imaging," *Appl. Phys. Lett.*, vol. 95, no. 13, pp. 131 110–1–131 110-3, 2009.

[8] H. Wang and S. S. Han, "Coherent ghost imaging based on sparsity constraint without phase-sensitive detection," *EPL*, vol. 98, no. 2, pp. 24 003–1–24 003-4, 2012.

[9] J. Cheng, "Ghost imaging through turbulent atmosphere," *Opt. Exp.*, vol. 17, no. 10, pp. 7916–7921, 2009.

[10] P. L. Zhang, W. L. Gong, X. Shen, and S. S. Han, "Correlated imaging through atmospheric turbulence," *Phys. Rev. A*, vol. 82, no. 3, pp. 033 817–1–033 817-4, 2010.

[11] W. L. Gong and S. S. Han, "Correlated imaging in scattering media," *Opt. Lett.*, vol. 36, no. 3, pp. 394–396, 2011.

[12] N. D. Hardy and J. H. Shapiro, "Reflective ghost imaging through turbulence," *Phys. Rev. A*, vol. 84, no. 6, pp. 063 824–1–063 824–12, 2011.

[13] D. F. Shi *et al.*, "Adaptive optical ghost imaging through atmospheric turbulence," *Opt. Exp.*, vol. 20, no. 27, pp. 27 992–27 998, 2012.

[14] H. Li, J. H. Shi, Y. C. Zhu, and G. H. Zeng, "Periodic diffraction correlation imaging through strongly scattering mediums," *Appl. Phys. Lett.*, vol. 103, no. 5, pp. 051 901–1–051 901-4, 2013.

[15] C. L. Luo and J. Cheng, "Ghost imaging with shaped incoherent sources," *Opt. Lett.*, vol. 38, no. 24, pp. 5381–5384, 2013.

[16] D. F. Shi *et al.*, "Two-wavelength ghost imaging through atmospheric turbulence," *Opt. Exp.*, vol. 21, no. 2, pp. 2050–2064, 2013.

[17] C. Zhang, W. L. Gong, and S. S. Han, "Improving imaging resolution of shaking targets by fourier-transform ghost diffraction," *Appl. Phys. Lett.*, vol. 102, no. 2, pp. 021 111–1–021 111-5, 2013.

[18] Z. W. Bo, W. L. Gong, and S. S. Han, "Motion de-blurring by second-order intensity-correlated imaging," *Chin. Opt. Lett.*, vol. 14, no. 7, pp. 070 301–1–070 301-4, 2016.

[19] R. H. Brown and R. Q. Twiss, "Correlation between photons in two coherent beams of light," *Nature*, vol. 177, pp. 27–32, 1956.

[20] G. Indebetouw and P. Klysubun, "Imaging through scattering media with depth resolution by use of low-coherence gating in spatiotemporal digital holography," *Opt. Lett.*, vol. 25, no. 4, pp. 212–214, 2000.

[21] E. N. Leith *et al.*, "Imaging through scattering media using spatial incoherence techniques," *Opt. Lett.*, vol. 16, no. 23, pp. 1820–1822, 1991.

[22] M. J. Kim, E. R. Mendez, and K. A. O'Donnell, "Scattering from gamma-distributed surfaces," *J. Mod. Opt.*, vol. 34, no. 8, pp. 1107–1119, 1987.

[23] J. W. Goodman, "Statistical properties of laser speckle patterns," in *Laser Speckle and Related Phenomena in Topics in Applied Physics*, vol. 9. Berlin, Germany: Springer-Verlag, 1975, p. 9.